Int. J. Solids Structures Vol. 30, No. 8, pp. 1015–1037, 1993
Printed in Great Britain

0020-7683/93 $6.00+ .00

A FINITE ELASTIC BODY WITH A CURVED CRACK LOADED IN ANTI-PLANE SHEAR

GLAUCIO H. PAULINO, MUHAMMED T. A. SAIF and SUBRATA MUKHERJEE
Department of Theoretical and Applied Mechanics, Cornell University, Ithaca, NY 14853, U.S.A.

(*Received* 4 *August* 1992; *in revised form* 4 *November* 1992)

Abstract—This paper presents a Boundary Integral Equation Method (BIEM) for an arbitrarily shaped, linearly elastic, homogeneous and isotropic body with a curved crack loaded in anti-plane shear. The crack must be modeled as an arc of a circle and wholly inside the solid—otherwise its position and orientation with respect to the boundary of the body is arbitrary.

The effect of the crack on the stress field is incorporated in an augmented kernel developed for the mode III crack problem such that discretization of the cutout boundary is no longer necessary. This modification of the kernel of the integral equation leads to solutions on and near the cutout with great accuracy. An asymptotic analysis is conducted in order to derive the Stress Intensity Factor (SIF) K_{III}, at each crack tip, in closed form. In this formulation, a straight crack can be viewed as a particular case of the more general curved crack. In particular, attention is paid to the influence of crack curvature and edge effect on the stress intensity factors at the right and left crack tips. A rigorous mathematical formulation is developed, the main aspects of the numerical implementation are discussed and several representative numerical examples are presented in this paper.

NOMENCLATURE

a, b	cutout or crack dimensions
B	body
BIEM	Boundary Integral Equation Method
CPV	Cauchy Principal Value
DLA	Direct Limit Approach
$F(Q)$	unknowns in the numerical method
h	relative size of the boundary element
H_{ij}, K	kernels
i	$\sqrt{-1}$
Im [·]	imaginary part of a complex variable
$k(\mathbf{A})$	condition number of a matrix $\mathbf{A}$
K_{III}	SIF for mode III crack
$K_{III\text{-}L}$	K_{III} at left crack tip
$K_{III\text{-}R}$	K_{III} at right crack tip
lim	limit
ln	natural logarithm
$\mathbf{n} = (n_1, n_2)$	unit outward normal
p, P	source point in B, or on ∂B, respectively
q, Q	field point in B, or on ∂B, respectively
r	distance (Euclidean norm)
Re [·]	real part of a complex variable
R_i, r_i	internal roots in the z plane
R_o, r_o	external roots in the z plane
s	distance measured along the boundary
SIF	Stress Intensity Factor
$\mathbf{t} = (t_1, t_2)$	unit anticlockwise tangent
x_1, x_2	Cartesian coordinates
z	complex variable in the physical plane
$\alpha, \beta, \gamma, \theta$	angles
Δx_1	distance from crack tip to a lateral edge
Δx_2	distance from crack to a parallel edge
λ	parameter that defines crack size and curvature
ξ	complex variable in the mapped plane
σ	stress tensor
τ	traction vector
τ_∞	remote applied uniform traction
ϕ	augmented kernel
$\hat{\phi}$	kernel for a simply-connected body
ϕ^*	kernel for an infinite body with a crack (or a cutout)

Φ	Airy stress function
(r, θ), (ε, α)	polar coordinates
∇^2	Laplacian operator
∂B	outer boundary of the body
∂B_2	crack or cutout boundary
$\sqrt{\cdot}$	square root
$\overline{(\cdot)}$, overbar	conjugate complex quantity
$(\cdot)'$, prime	derivative with respect to argument
$\|\cdot\|$	absolute value
$\|\mathbf{A}\|$	norm of a matrix $\mathbf{A}$
$\odot$	axis oriented out of the plane of the paper
$\oplus$	axis pointing to the plane of the paper.

1. INTRODUCTION

The mode III fracture mechanics problem in a linearly elastic solid has been a subject of research for many years. Historically, the study of the anti-plane crack problem (governed by the harmonic operator) has been the basis for the understanding of the opening mode crack problem (governed by the bi-harmonic operator). Several numerical and analytical solutions have been proposed for the anti-plane crack problem. Sih (1965) and Chiang (1987) have proposed analytical solutions for mode III curved cracks in infinite regions. Zhang (1987, 1989), Ma (1988) and Ma and Zhang (1991) have proposed analytical solutions for mode III straight cracks in finite regions. There exist some papers that address the problem of curved cracks in finite regions by the Boundary Integral Equation Method (BIEM) considering modes I and II (Blandford *et al.*, 1981; Zhang and Gudmundson, 1988; Liu *et al.*, 1990) or mode III (Liu and Altiero, 1992). However, to the best of the authors' knowledge, there is no published solution for the problem of a curved crack in a finite region without having to model the crack surface explicitly in a numerical procedure. This is the subject of this paper.

Sih (1965) has developed analytical solutions for the mode III Stress Intensity Factors (SIFs) of several crack configurations in infinite regions. Chiang (1987) has proposed an integral equation for the mode III of a slightly curved crack in an infinite region using perturbation procedures similar to those carried out for the in-plane loading case by Cotterell and Rice (1980). Some recent papers have been published on analytical solutions for mode III SIFs considering a finite region with an eccentric straight crack, e.g. Zhang (1987, 1989) and Ma and Zhang (1991). Ma (1988) has used Fourier transforms and Fourier series to find the mode III SIF for a central crack in a rectangular sheet, where its boundary is subjected to an arbitrary anti-plane load.

Mews and Kuhn (1988) have used Green's functions, for both the central and the semi-infinite traction-free straight crack in an isotropic elastic material, to derive boundary integral equations for SIFs for in-plane and anti-plane states of strain. They have used the Direct Boundary Integral Equation Method to determine the SIFs based on the asymptotic displacement field at the tips of a straight crack. The Indirect Boundary Integral Equation Method has been used to solve fracture problems by Sadegh and Altiero (1979) and Mukherjee (1982). The former authors used displacement-based formulations while Mukherjee (1982) used stress-based formulations.

A new efficient and accurate solution procedure, based on the BIEM, is proposed here for the problem of a finite elastic solid, with a curved crack, loaded in anti-plane shear. The body is of arbitrary shape and is linearly elastic, homogeneous and isotropic. The crack must be an arc of a circle and wholly inside the solid—otherwise, its position and orientation with respect to the boundary of the body is arbitrary. The elasticity solution makes use of complex variables for the analytical treatment of the problem. The singular kernels for an infinite domain are augmented such that the new kernels are singular solutions for a point source in an infinite domain containing a traction-free curved crack modeled as an arc of a circle. This analysis technique leads to a very effective numerical procedure for the stress analysis of a cracked body where crack discretization is not necessary. All the unknowns of the problem lie only on the outer boundary of the body. A complex variable boundary integral equation is derived for determining these boundary unknowns. A mode III SIF is obtained by an asymptotic analysis of the stress field as a crack tip is approached. An

integral expression for the SIFs at each crack tip is also derived. In contrast to the work of Mews and Kuhn (1988) on straight cracks, the determination of the SIFs in this paper is concerned with asymptotic stress fields at the tips of a curved crack.

2. DIFFERENTIAL EQUATIONS FOR THE ANTI-PLANE STRAIN STATE

Consider a body B loaded in anti-plane shear. Assume the x_1 and x_2 axes in the plane defined by the cross-section of the body and the x_3 axis normal to it. The only nonzero stress components are $\sigma_{31}(=\sigma_{13})$ and $\sigma_{32}(=\sigma_{23})$ given by

$$\sigma_{31} = \frac{\partial \Phi(x_1, x_2)}{\partial x_2}, \quad \sigma_{32} = -\frac{\partial \Phi(x_1, x_2)}{\partial x_1}, \tag{1}$$

where $\Phi(x_1, x_2)$ is the Airy stress function of the problem. It satisfies Laplace's equation:

$$\nabla^2 \Phi = 0, \tag{2}$$

where ∇^2 is the Laplacian operator in two dimensions.

Only Neuman boundary conditions are considered in the present analysis. The traction $\tau_3 \equiv \tau$ at any point of the boundary ∂B is

$$\tau = \sigma_{3i} n_i = \frac{\partial \Phi}{\partial x_2} n_1 - \frac{\partial \Phi}{\partial x_1} n_2 = \frac{\partial \Phi}{\partial x_i} t_i = \frac{\partial \Phi}{\partial s}, \tag{3}$$

where $\mathbf{n} = (n_1, n_2)$ and $\mathbf{t} = (t_1, t_2)$ are the unit outward normal and unit anticlockwise tangent vectors, respectively, at a point on the boundary ∂B; s is the distance measured along a boundary in an anticlockwise sense and $(\partial \Phi / \partial s)$ is the tangential derivative of the stress function.

3. INDIRECT BOUNDARY INTEGRAL EQUATION METHOD FORMULATIONS

First, an Indirect Boundary Integral Equation Method formulation for a simply-connected body (Section 3.1) is developed by means of the real variables theory. Next, this formulation is revisited to formulate the problem of a body with cutout (Section 3.2) by means of the complex variables theory.

3.1. *Simply-connected body*

Consider a body B loaded in anti-plane shear as illustrated by Fig. 1. The Laplace equation (2) can be transformed into an integral equation by using a single layer potential (Mukherjee, 1982) such that

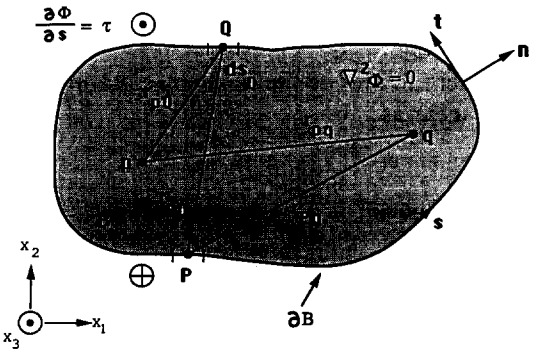

Fig. 1. Cross-section of a body loaded in anti-plane shear.

$$2\pi\Phi(p) = \int_{\partial B} \ln r_{pQ} F(Q)\, ds_Q, \tag{4}$$

where F is the boundary density function to be determined from the boundary conditions, r is the distance between the source point p (or P) and the field point q (or Q), where lower case letters denote points inside the body B and capital letters denote points on its boundary ∂B (see Fig. 1).

Differentiating eqn (4) with respect to x_j ($j = 1, 2$) and making use of eqn (1), the integral equation for internal stresses is obtained as

$$2\pi\sigma_{3j}(p) = \int_{\partial B} H_{3j}(p, Q) F(Q)\, ds_Q, \tag{5}$$

where

$$H_{31}(p, Q) = \frac{\partial \phi}{\partial x_2}, \quad H_{32}(p, Q) = -\frac{\partial \phi}{\partial x_1}, \quad \phi = \ln r_{pQ}. \tag{6}$$

The integral equation for the boundary stresses can be derived by taking the limit as $p \to P$ of eqn (5) to obtain

$$2\pi\sigma_{3j}(P) = \int_{\partial B} H_{3j}(P, Q) F(Q)\, ds_Q + \pi t_j(P) F(P), \tag{7}$$

where the boundary ∂B is considered to be locally smooth at the source point P.

The traction for a point P on ∂B where ∂B is locally smooth can be derived by taking the dot product of both sides of eqn (7) with $n_j(P)$ and making use of the first equality on eqn (3):

$$2\pi\tau(P) = \int_{\partial B} H_{3j}(P, Q) n_j(P) F(Q)\, ds_Q. \tag{8}$$

The singular integrals in eqns (7) and (8) can be interpreted in the CPV (Cauchy Principal Value) sense.

3.2. *Body with cutout*

The idea here is to augment the previous kernel for the simply-connected body such that it includes the effect of the cutout, and therefore discretization of the cutout boundary becomes unnecessary. For this purpose, the complex variable approach (Muskhelishvili, 1963) is used to formulate the elasticity problem using an augmented kernel for a body with a cutout (Mukherjee, 1982).

Therefore, it is convenient to rewrite the elasticity equation (4) for a simply-connected body loaded in anti-plane shear as:

$$2\pi\Phi(p) = \int_{\partial B} K(p, Q) F(Q)\, ds_Q, \tag{9}$$

where

$$K(p, Q) = \mathrm{Re}\,\{\hat{\phi}(z, z_0)\} \tag{10}$$

and

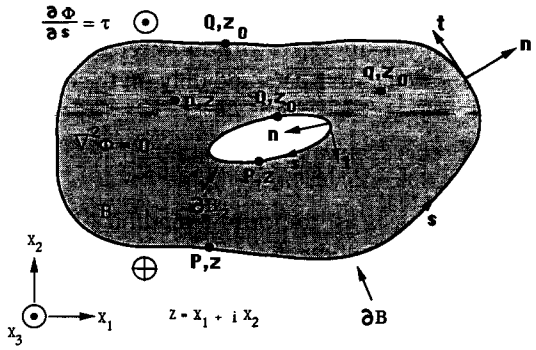

Fig. 2. Body with cutout loaded in anti-plane shear.

$$\hat{\phi}(z, z_0) = \ln(z - z_0). \tag{11}$$

Here Re denotes the real part of the complex function and z, z_0 are the source and field points, respectively, in the complex plane.

Consider a body, with a traction free cutout, subjected to an anti-plane shear loading, as shown in Fig. 2. Define a function $\phi^*(\cdot)$ of z, z_0, and significant variables that describe the cutout geometry. The function $\phi^*(\cdot)$, associated with the cutout, must satisfy the following properties

- $\phi^*(\cdot)$ satisfies Laplace's equation.
- $\phi^*(\cdot)$ is regular outside the cutout boundary ∂B_2.
- $\phi(z, \bar{z}, z_0, \cdot) = \hat{\phi}(z, z_0) + \phi^*(\cdot)$ vanishes on the cutout boundary ∂B_2.

Box 1. Properties of the augmented kernel.

The kernel $\hat{\phi}$ generates stresses in the simply-connected body. The kernel ϕ^* releases stresses from the cutout boundary. Together, the augmented kernel $\phi = \hat{\phi} + \phi^*$ enforces the traction free boundary condition along the cutout contour.

As a simple example, suppose that the cutout in Fig. 2 is the unit circle $|z| = 1$. For this case, the kernels ϕ^* and ϕ are:

$$\phi^*(\bar{z}, z_0) = -\ln\left(\frac{1}{\bar{z}} - z_0\right), \tag{12}$$

$$\phi(z, \bar{z}, z_0) = \ln(z - z_0) - \ln\left(\frac{1}{\bar{z}} - z_0\right). \tag{13}$$

One can verify that the above equations satisfy the required properties for the augmented kernel stated in Box 1.

The boundary integral equations for internal stresses, boundary stresses and tractions have the same forms as eqns (5), (7) and (8), respectively. However, the augmented kernels H_{3j} must be redefined as:

$$H_{31} = \mathrm{Re}\left[\frac{\partial \phi}{\partial x_2}(z, \bar{z}, z_0, \cdot)\right] = \mathrm{Im}\left[\frac{\partial \phi}{\partial \bar{z}} - \frac{\partial \phi}{\partial z}\right], \tag{14}$$

$$H_{32} = -\mathrm{Re}\left[\frac{\partial \phi}{\partial x_1}(z, \bar{z}, z_0, \cdot)\right] = -\mathrm{Re}\left[\frac{\partial \phi}{\partial z} + \frac{\partial \phi}{\partial \bar{z}}\right], \tag{15}$$

where Im denotes the imaginary part of the complex function.

The use of the augmented kernel technique leads to a powerful formulation where the mechanical behavior of the body is obtained without discretizing the cutout boundary ∂B_2 shown in Fig. 2. The boundary elements are needed only on the outer boundary ∂B (Fig. 2).

4. CONFORMAL MAPPING

Applied conformal mapping is an important method of analysis in many technical areas such as mechanics, physics, heat flow, fluid flow, computer graphics, electromagnetics and acoustics. The main idea consists of using functions of complex variables to transform complicated boundaries into simpler ones. Recently, Schinzinger and Laura (1991) have published a comprehensive book about conformal mapping, with numerous applications.

The elasticity solution for a body with a cutout has been formulated by means of functions of complex variables. In order to derive the function ϕ^* for generic shapes of the cutout boundary, it is advantageous to make use of conformal mapping to transform the region on and outside the cutout in the z plane to the region on and inside a unit circle in the ξ plane. This transformation needs to be done rigorously because any approximation on the cutout modeling will affect the fundamental kernel ϕ that describes the mechanical behavior of the body.

Mukherjee (1982) has studied plates with elliptical cutouts and straight cracks. He has used conformal mapping to transform an ellipse, in the z plane, to a circle in the ξ plane. The mapping function is:

$$z = f(\xi) = \left(\frac{a-b}{2}\right)\xi + \left(\frac{a+b}{2}\right)\frac{1}{\xi}, \tag{16}$$

where a and b are the semi-major and semi-minor axes of the ellipse, respectively. The crack is modeled by taking the limit of eqn (16) as $b \to 0$.

The fundamental problem here consists of finding an analytic function $z = f(\xi)$ that conformally maps the region on and outside a crack having the shape of an arc of a circle in the z plane, to the region on and inside a unit circle in the ξ plane. The Riemann Mapping Theorem guarantees that this conformal mapping exists, although the theorem provides no assistance in finding a suitable transformation. The proof of this theorem can be found in many books about Complex Variables [for example, Dettman (1984), Theorem 6.4.7].

A sequence of three mappings will be used to obtain the required mapping function. These mappings are illustrated in Fig. 3. The bilinear transformation between the z and z_1 planes is:

$$z_1 = \frac{1-i\lambda}{1+i\lambda}\frac{z+1}{z-1}, \tag{17}$$

where the parameter λ uniquely determines the size and curvature of the arc of a circle. The transformation between the z_1 and z_2 planes is:

$$z_2 = \sqrt{z_1}. \tag{18}$$

In this case, the mapping of the arc of a circle in the z_1 plane, i.e. the real negative axis of the z_1 plane, can be taken as a branch cut for the evaluation of the complex square root function. Finally, the bilinear transformation between the z_2 and ξ planes is:

$$\xi = \frac{z_2-1}{z_2+1}. \tag{19}$$

Substitution of eqns (18) and (17) into eqn (19) leads to the mapping function:

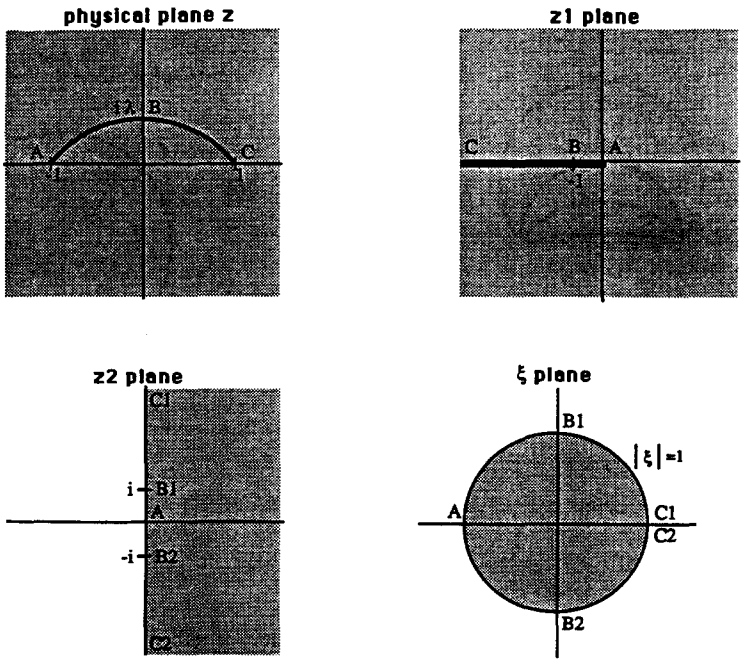

Fig. 3. Steps to map an arc of a circle (z plane) onto a unit circle (ξ plane).

$$\xi(z,\lambda)=\frac{\sqrt{(1-i\lambda)(z+1)}-\sqrt{(1+i\lambda)(z-1)}}{\sqrt{(1-i\lambda)(z+1)}+\sqrt{(1+i\lambda)(z-1)}}. \tag{20}$$

This mapping takes any point in the z plane to two points in the ξ plane, one of which is within the unit circle and the other one is outside the unit circle. The mapping is conformal, except at the crack tips. Note that conformality does not require that the Laplacian operator of eqn (2) be satisfied at all points on the boundary of the region in the z plane (Fig. 3) (Greenberg, 1978, pp. 291–293).

Here, the inverse mapping maps the region on and inside a unit circle in the ξ plane, to the region on and outside a crack having the shape of an arc of a circle in the z plane (Fig. 3). The inverse mapping $z(\xi, \lambda)$ exists [see Dettman (1984), Theorem 6.4.8] and is given by

$$z(\xi,\lambda)=\frac{(1+i\lambda)(1+\xi)^2+(1-i\lambda)(1-\xi)^2}{(1+i\lambda)(1+\xi)^2-(1-i\lambda)(1-\xi)^2}. \tag{21}$$

Application of eqns (20) and (21) is shown in Fig. 4 for several values of λ: 0.1 (slightly curved crack), 0.5, 1.0 (semi-circle) and 2.0. The real axis inside the unit circle in the ξ plane is mapped onto a circular arc in the z plane. The imaginary axis inside the unit circle in the ξ plane is mapped onto a segment of the imaginary line in the z plane.

Notice that the upper half circle in the ξ plane (arc AB_1C_1 in Fig. 3) and its conjugate points represented by the lower half circle in the ξ plane (arc AB_2C_2 in Fig. 3) are mapped onto exactly the same positions in the z plane (see Fig. 4). This property is defined here as *symmetric mapping*. It ensures the exact mathematical representation of a crack in the shape of an arc of a circle. Physically, this means that the crack surface discontinuity (i.e. two surfaces occupying the same location) for the planar ($\lambda = 0$) or non-planar ($\lambda \neq 0$) crack is actually modeled by the present formulation.

5. FORMULATION FOR A FINITE BODY WITH A CURVED CRACK

This section presents the kernels for a body with an internal crack loaded in anti-plane shear. The crack is modeled as an arc of a circle. Using these kernels, an asymptotic analysis

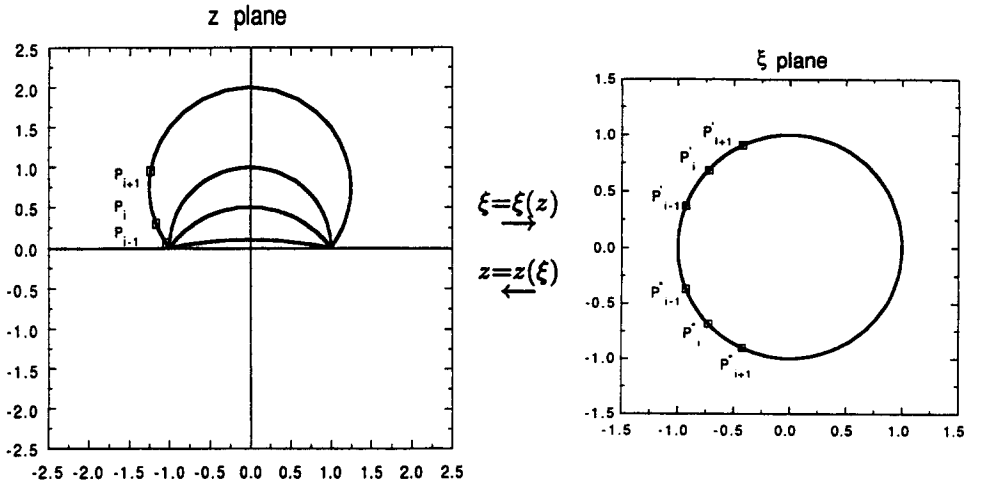

Fig. 4. Conformal mapping for several values of λ.

of the near tip stress field is conducted in order to derive a boundary integral expression for the stress intensity factor (K_{III}).

5.1. *Augmented kernels*

The function $\hat{\phi}$ for a body with a curved crack is derived by making use of the conformal mapping given by eqns (20) and (21). Substitution of eqn (21) into eqn (11) leads to:

$$\hat{\phi} = \ln(z-z_0) = \ln\left[\frac{(\xi-R_i)(\xi-R_o)(1-i\lambda z_0)}{(\xi-r_i)(\xi-r_o)\,i\lambda}\right], \tag{22}$$

where

$$R_i(z_0,\lambda) = \frac{z_0 - i\lambda - \sqrt{(1-\lambda^2)(z_0^2-1)}}{1-i\lambda z_0}, \quad |R_i| \leqslant 1, \tag{23}$$

$$R_o(z_0,\lambda) = \frac{1}{R_i}, \quad |R_o| \geqslant 1, \tag{24}$$

$$r_i(\lambda) = i\left(\frac{1-\sqrt{1+\lambda^2}}{\lambda}\right), \quad |r_i| \leqslant 1, \tag{25}$$

$$r_o(\lambda) = \frac{1}{r_i}, \quad |r_o| \geqslant 1, \tag{26}$$

with $\lambda > 0$. R_i and R_o are the roots of $z - z_0 = 0$ in the ξ plane. r_i and r_o are the mapped points of $z = \infty$. When $\lambda \to 0$, $r_i \to 0$ and r_o is unbounded in the imaginary axis on the ξ plane. Moreover, it can be shown that

$$R_i(z_0,\lambda) = \xi(z_0,\lambda). \tag{27}$$

Equation (22) can have singularities at $\xi = R_i$ and $\xi = r_i$ inside the unit circle $|\xi| = 1$. A straight crack implies $r_i = 0$. The function ϕ^*, satisfying the conditions in Box 1, is chosen in a manner analogous to the straight crack as derived by Mukherjee (1982). The result is

$$\phi^*(z,\bar{z},z_0,\lambda)=\ln\left[\frac{(\xi-r_o)(1-r_i\bar{\xi})\,i\lambda}{(\xi-R_o)(1-R_i\bar{\xi})(1-i\lambda z_0)}\right], \tag{28}$$

such that

$$\phi(z,\bar{z},z_0,\lambda)=\hat{\phi}+\phi^*=\ln\left[\frac{(\xi-R_i)(1-r_i\bar{\xi})}{(\xi-r_i)(1-R_i\bar{\xi})}\right] \tag{29}$$

is the resultant potential for the body with a curved crack in the shape of an arc of a circle. This function vanishes on the unit circle $|\xi|=1$ and therefore it also vanishes on the corresponding curved crack in the z plane. The other properties for the augmented kernel stated in Box 1 are also satisfied.

Taking the limit of $\phi(z,\bar{z},z_0,\lambda)$ on eqn (29) as $\lambda\to 0$, it can be verified that the kernel function $\phi(z,\bar{z},z_0)$ for a line crack derived by Mukherjee (1982, p. 154) is recovered as a particular case of the present formulation. This verification shows the consistency of the present formulation.

5.2. *Asymptotic analysis for the stress intensity factors*

Asymptotic analysis is a branch of mathematics dedicated to the study of the behavior of functions in particular limits of interest (Erdélyi, 1956). Here, the interest is to study the behavior of the stress field in the vicinity of the tips of a curved crack modeled as an arc of a circle.

When the notch is a sharp crack, the near tip stress field from a linear elastic analysis in the case of anti-plane loading is given by

$$\sigma_{3j}\to\frac{K_{III}}{\sqrt{2\pi r}}f_{3j}(\theta), \tag{30}$$

where (r,θ) represent polar coordinates as shown in Fig. 5 and $f_{3j}(\theta)$ expresses the angular distribution of the singular stress field. In this case, the resulting stresses can be found in many books and papers about fracture mechanics [for example Rice (1968)]:

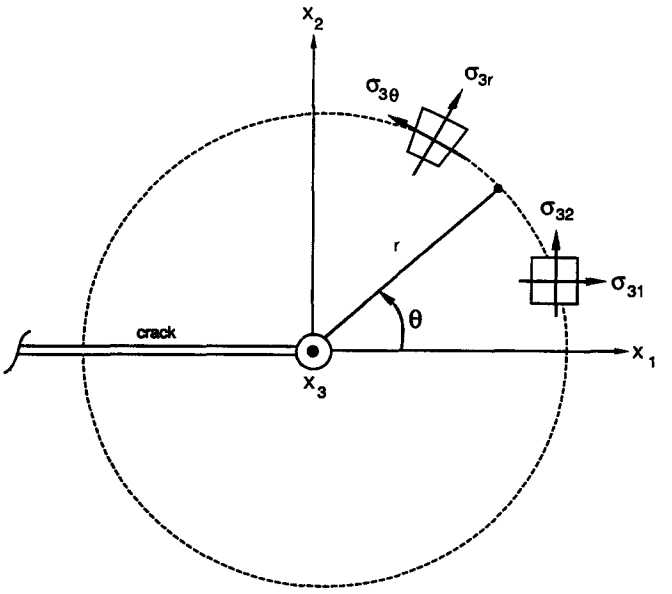

Fig. 5. Rectangular and polar stress components for the anti-plane crack problem.

$$\begin{Bmatrix}\sigma_{31}\\ \sigma_{32}\end{Bmatrix} = \frac{K_{III}}{\sqrt{2\pi r}}\begin{Bmatrix}-\sin(\theta/2)\\ \cos(\theta/2)\end{Bmatrix}. \tag{31}$$

Equation (30) is useful for the derivation of closed form equations for K_{III}. For instance, consider first the determination of the stress intensity factor at the right crack tip, denoted by $K_{III\text{-}R}$. Taking into account the form of the kernel function ϕ in eqn (29), it is convenient to use the chain rule to rewrite eqn (14) as

$$H_{31} = \mathrm{Re}\left[\frac{\partial\phi}{\partial x_2}(z,\bar{z},z_0,\lambda)\right] = \mathrm{Re}\left[\frac{\partial\phi}{\partial\xi}\frac{\partial\xi}{\partial z}\frac{\partial z}{\partial x_2} + \frac{\partial\phi}{\partial\bar{\xi}}\frac{\partial\bar{\xi}}{\partial\bar{z}}\frac{\partial\bar{z}}{\partial x_2}\right], \tag{32}$$

such that

$$H_{31} = \mathrm{Re}\left[\mathrm{i}\left(\frac{1}{\xi-R_i} - \frac{1}{\xi-r_i}\right)\xi' - \mathrm{i}\left(\frac{R_i}{1-R_i\bar{\xi}} - \frac{r_i}{1-r_i\bar{\xi}}\right)\bar{\xi}'\right], \tag{33}$$

where

$$\xi' = \frac{\partial\xi}{\partial z} \quad \text{and} \quad \bar{\xi}' = \frac{\partial\bar{\xi}}{\partial\bar{z}}. \tag{34}$$

Equation (33) can be rearranged in the following form:

$$H_{31} = \mathrm{Re}\left\{\mathrm{i}\left[\frac{1}{(1-R_i)\left(1+\dfrac{\xi-1}{1-R_i}\right)} - \frac{1}{(1-r_i)\left(1+\dfrac{\xi-1}{1-r_i}\right)}\right]\xi' - \mathrm{i}\left[\frac{R_i}{(1-R_i)\left(1-\dfrac{R_i(\bar{\xi}-1)}{1-R_i}\right)} - \frac{r_i}{(1-r_i)\left(1-\dfrac{r_i(\bar{\xi}-1)}{1-r_i}\right)}\right]\bar{\xi}'\right\}. \tag{35}$$

Now, eqn (35) can be expressed in terms of an infinite series:

$$H_{31} = \mathrm{Re}\left\{\mathrm{i}\left[\frac{1}{1-R_i}\left(1-\frac{\xi-1}{1-R_i}+\cdots\right) - \frac{1}{1-r_i}\left(1-\frac{\xi-1}{1-r_i}+\cdots\right)\right]\xi' - \mathrm{i}\left[\frac{R_i}{1-R_i}\left(1+\frac{\bar{\xi}-1}{1-R_i}R_i+\cdots\right) - \frac{r_i}{1-r_i}\left(1+\frac{\bar{\xi}-1}{1-r_i}r_i+\cdots\right)\right]\bar{\xi}'\right\}. \tag{36}$$

Note that the higher order terms of the near tip stress field can be obtained by adding higher order terms in each Taylor series expansion of eqn (36). Each series in eqn (36) has the form of the well-known geometric series. In the present case, each of the above series converges because as $\xi \to 1$,

$$\left|\frac{\xi-1}{1-R_i}\right| \ll 1 \quad \text{and} \quad \left|\frac{\xi-1}{1-r_i}\right| \ll 1 \tag{37}$$

and also, as $\bar{\xi} \to 1$,

$$\left|\frac{\bar{\xi}-1}{1-R_i}R_i\right| \ll 1 \quad \text{and} \quad \left|\frac{\bar{\xi}-1}{1-r_i}r_i\right| \ll 1. \tag{38}$$

Applying asymptotic analysis, a first order approximation for H_{31} around the right crack tip leads to

$$\begin{aligned}\lim_{\xi,\bar{\xi};z,\bar{z}\to 1} H_{31} &= \mathrm{Re}\left[\mathrm{i}\left(\frac{1}{1-R_i}-\frac{1}{1-r_i}\right)\xi' - \mathrm{i}\left(\frac{R_i}{1-R_i}-\frac{r_i}{1-r_i}\right)\bar{\xi}'\right] \\ &= \mathrm{Re}\left[\mathrm{i}\left(\frac{1}{1-R_i}-\frac{1}{1-r_i}\right)(\xi'-\bar{\xi}')\right] \\ &= -\mathrm{Re}\left\{\left(\frac{1}{1-R_i}-\frac{1}{1-r_i}\right)2\,\mathrm{Im}\left[\lim_{z\to 1}\xi'\right]\right\},\end{aligned} \tag{39}$$

where the derivative of the function ξ in the close neighborhood of the right crack tip can be obtained from eqn (20) as

$$\begin{aligned}\lim_{z\to 1}\xi' &= -\lim_{z\to 1}\sqrt{\frac{1+\mathrm{i}\lambda}{1-\mathrm{i}\lambda}}\frac{1}{\sqrt{(z+1)(z-1)}} \\ &= -\sqrt{\frac{1+\mathrm{i}\lambda}{1-\mathrm{i}\lambda}}\frac{1}{\sqrt{2\varepsilon}}\mathrm{e}^{-\mathrm{i}(\alpha/2)} \\ &= -\frac{1}{\sqrt{2\varepsilon}}\mathrm{e}^{\mathrm{i}(\tan^{-1}\lambda-(\alpha/2))},\end{aligned} \tag{40}$$

in which (ε, α) represent polar coordinates with respect to the local coordinate system at the crack tip considering the curved configuration, as shown in Fig. 6, and ε is a small radius from the crack tip and inside the K_{III} dominant region (see Fig. 5). Substitution of eqn (40) in eqn (39) gives

$$\lim_{\xi,\bar{\xi};z,\bar{z}\to 1} H_{31} = \mathrm{Re}\left\{2\left(\frac{1}{1-R_i}-\frac{1}{1-r_i}\right)\mathrm{Im}\left[\frac{1}{\sqrt{2\varepsilon}}\mathrm{e}^{\mathrm{i}(\tan^{-1}\lambda-(\alpha/2))}\right]\right\}. \tag{41}$$

The dominant singular term of stresses as the crack tip is approached can be obtained from an appropriate limiting form of the boundary integral equation (5). For the present case

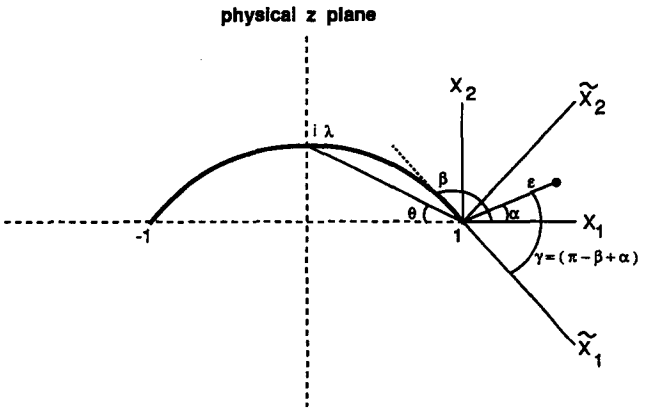

Fig. 6. Local coordinate systems at the right crack tip.

$$\lim_{\xi,\bar{\xi};z,\bar{z}\to 1}\sigma_{31}=\frac{1}{2\pi}\lim_{\xi,\bar{\xi};z,\bar{z}\to 1}\int_{\partial B}H_{31}(p,Q)F(Q)\,\mathrm{d}s_Q \tag{42}$$

and the use of a Direct Limit Approach (DLA) leads to:

$$\lim_{\xi,\bar{\xi};z,\bar{z}\to 1}\sigma_{31}=\frac{1}{2\pi}\int_{\partial B}\left[\lim_{\xi,\bar{\xi};z,\bar{z}\to 1}H_{31}(p,Q)\right]F(Q)\,\mathrm{d}s_Q. \tag{43}$$

Substitution of eqn (41) in eqn (43) yields

$$\lim_{\xi,\bar{\xi};z,\bar{z}\to 1}\sigma_{31}=\frac{K_{\text{III-R}}}{\sqrt{2\pi\varepsilon}}\,\mathrm{Im}\,[\mathrm{e}^{\mathrm{i}(\tan^{-1}\lambda-(\alpha/2))}], \tag{44}$$

where

$$K_{\text{III-R}}=\frac{1}{\sqrt{\pi}}\left[-\mathrm{Re}\left(\frac{1}{1-r_{\mathrm{i}}(\lambda)}\right)\int_{\partial B}F(Q)\,\mathrm{d}s_Q+\int_{\partial B}\frac{1}{1-\xi(z_0,\lambda)}F(Q)\,\mathrm{d}s_Q\right]. \tag{45}$$

Note that the above formula for $K_{\text{III-R}}$ involves quantities on the outer boundary and none in the immediate vicinity of the crack tip. It is expected that quantities reasonably remote from the crack tip can be calculated much more accurately from a numerical method involving eqn (5) than those quantities very near the crack tip.

Similar derivations for the internal stress σ_{32} around the right crack tip lead to

$$\lim_{\xi,\bar{\xi};z,\bar{z}\to 1}\sigma_{32}=\frac{K_{\text{III-R}}}{\sqrt{2\pi\varepsilon}}\,\mathrm{Re}\,[\mathrm{e}^{\mathrm{i}(\tan^{-1}\lambda-(\alpha/2))}]. \tag{46}$$

The advantage of elastic stress analysis lies in the similarity of near crack tip stress distributions for all configurations. Therefore, it must be shown that the fundamental stress field in eqn (31) can be recovered from the stress field in eqns (44) and (46).

Consider Fig. 6 again and define the analytic function away from the tips

$$\sigma(z)=\sigma_{3\tilde{2}}+\mathrm{i}\sigma_{3\tilde{1}}. \tag{47}$$

Therefore,

$$\begin{aligned}\sigma_{3\tilde{1}}&=\mathrm{Im}\,[\sigma\,\mathrm{e}^{\mathrm{i}(\beta-\pi)}],\\ \sigma_{3\tilde{2}}&=\mathrm{Re}\,[\sigma\,\mathrm{e}^{\mathrm{i}(\beta-\pi)}],\end{aligned} \tag{48}$$

where $(\tilde{x}_1,\tilde{x}_2)$ represent the local Cartesian system at the right crack tip considering the curved crack configuration and the angle β is shown in Fig. 6. Substitution of eqns (44) and (46) in eqn (47) gives:

$$\sigma=\frac{K_{\text{III-R}}}{\sqrt{2\pi\varepsilon}}\,\mathrm{e}^{\mathrm{i}(\tan^{-1}\lambda-(\alpha/2))}. \tag{49}$$

From geometry,

$$\tan^{-1}\lambda=\frac{\pi-\beta}{2}. \tag{50}$$

Substitution of eqns (49) and (50) into eqns (47) and (48) gives

$$\begin{Bmatrix}\sigma_{3\hat{r}}\\ \sigma_{3\hat{z}}\end{Bmatrix} = \frac{K_{\text{III-R}}}{\sqrt{2\pi\varepsilon}}\begin{Bmatrix}-\sin(\gamma/2)\\ \cos(\gamma/2)\end{Bmatrix}, \quad \gamma = \pi-\beta+\alpha, \tag{51}$$

which is analogous to eqn (31), as expected. This is a verification of the "Autonomy Concept" [see, for example, Freund (1990)] in Fracture Mechanics.

Analogous derivations for the left crack tip permit one to derive a closed form boundary integral equation for the stress intensity factor similar to eqn (45):

$$K_{\text{III-L}} = \frac{1}{\sqrt{\pi}}\left[-\text{Re}\left(\frac{1}{1+r_i(\lambda)}\right)\int_{\partial B} F(Q)\,ds_Q + \int_{\partial B}\frac{1}{1+\xi(z_0,\lambda)}F(Q)\,ds_Q\right] \tag{52}$$

in which $K_{\text{III-L}}$ is the stress intensity factor at the left crack tip. A discussion of K_{III} at the left and right crack tips is given in the Appendix.

6. NUMERICAL ASPECTS

A BIEM program has been developed to perform stress analysis of finite elastic bodies with internal curved cracks loaded in anti-plane shear. In order to develop a simple computer code, the numerical part of this paper uses discretization of the integral equations in terms of real variables theory. However, the theoretical part of this paper is based on complex variables theory.

Due to the robustness of the mathematical formulation developed, a simple numerical technique is used in which the concentrations $F(Q)$ in eqn (5) are assumed to be piecewise uniform on each boundary segment with their values assigned at nodes located at the centers of each segment. Procedures for numerical discretization of the boundary integral equations (5), (7) and (8) can be found in Mukherjee (1982).

Two techniques of integration have been used: numerical and analytical. Numerical integration uses 4 point Gauss quadrature. Analytical integration has been used to integrate the singular kernel in the CPV sense, and also to integrate the regular integrals in closed form whenever possible.

The solution of the linear equation system uses Gauss–Jordan elimination with full pivoting. The condition number of the system matrix [see, for example, Golub and Van Loan (1989)] can also be evaluated. Let $\mathbf{A} = [a_{ij}]$ be a nonsingular matrix of order n. Here, the condition number is defined as

$$k(A) = \|A\|\,\|A^{-1}\|, \tag{53}$$

where the norm of the matrix A is defined as

$$\|A\| = \left[\sum_{i=1}^{n}\sum_{j=1}^{n} a_{ij}^2\right]^{1/2}. \tag{54}$$

7. EXAMPLES

In order to assess the effectiveness of the proposed formulation, the following examples are presented:

(1) h-convergence verification;
(2) Numerical simulation of an infinite cracked body;
(3) Curved crack in an infinite body;
  (3.1) Effect of crack curvature;
  (3.2) Effect of curved crack orientation;
(4) Symmetric edge effect;
  (4.1) Crack tips approaching perpendicular edges;
  (4.2) A crack approaching a parallel edge;
(5) Nonsymmetric edge effect.

The purpose of the first two examples is to validate the proposed formulation and to gain initial understanding about the numerical method. Examples (3) and (4) focus on important problems for which analytical solutions are available. Example (5) only presents the solution from the proposed numerical method because no analytical solution considering non-symmetric edge effects is available. Uniform discretization of the outer boundary (∂B) of the body (Fig. 2), in the physical plane, is used for all the examples. There is no need to discretize the crack faces (∂B_2) because their effect is included in the kernel of the mathematical formulation. All the computations in this work have been executed in a VAX station 3100.

7.1. h-*convergence verification*

The objective of the first example is to perform a h-convergence study to validate the present formulation. The problem to be considered is that of a straight crack of length $2a$ in an infinite body subjected to an out-of-plane shear stress τ_∞ at infinity. The tearing mode stress intensity factor for an infinite body with a straight crack is defined as

$$K_{\mathrm{III}} = \tau_\infty \sqrt{\pi a}. \tag{55}$$

In the present example, the cross-section of the body is modeled as a square plate of length $2L$. The plate size is chosen such that $L/a = 20$. Uniform discretization of the plate boundary is adopted here and h is defined as the relative size of the boundary element, i.e.

$$h = \frac{\text{actual length of a boundary element}}{L}. \tag{56}$$

Therefore, $1/h$ is the number of elements along each edge of the plate. The discretization is defined as odd or even if the number $1/h$ is odd or even, respectively.

Figure 7 shows the results of the h-convergence study considering even discretization. It can be observed that the numerical values converge monotonically to the analytical result in this case.

A faster rate of convergence is observed when using odd discretization. The graph in Fig. 8 shows the results of the h-convergence study considering both even and odd discretization. The numerical results converge to the analytical one, but not monotonically. This type of oscillatory convergence is not uncommon for the boundary element method.

A complete proof of convergence of the numerical solutions is beyond the scope of this work. The interested reader is referred to, for example, Ghosh (1982) and Sloan (1991), for proofs of convergence of numerical solutions of the BIEM equations for potential

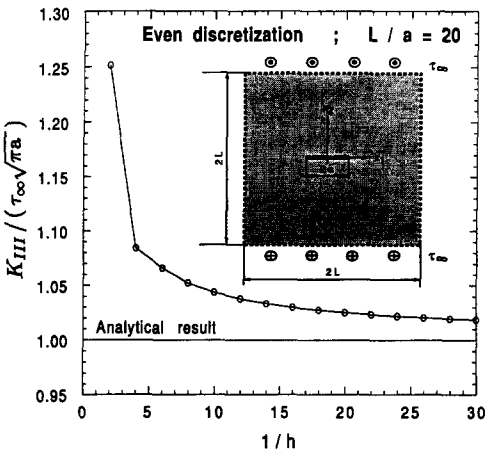

Fig. 7. h-convergence considering even discretization.

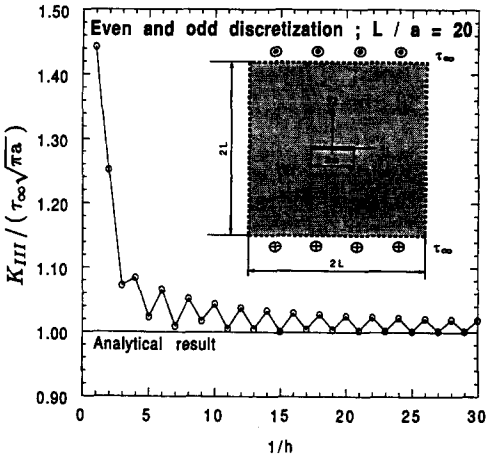

Fig. 8. h-convergence considering even and odd discretization.

problems (Laplace's equation). Perhaps these proofs can be extended in the future to include corners on the outer boundary of a body and a crack inside it.

7.2. *Numerical simulation of an infinite cracked body*

This example consists of determining the size of the plate, within acceptable numerical error limits, required to eliminate the effect of the boundary on the stress intensity factors. Two different uniform discretizations with $1/h = 15$ and $1/h = 20$ are used for all the meshes. The results are presented in Table 1, where the relative error on the stress intensity factor K_{III} is defined as:

$$\text{Error in } K_{III} = \left(\frac{K_{III}(\text{BIEM})}{K_{III}(\text{Analytical})} - 1 \right) 100\%, \tag{57}$$

where the analytical solution for this example is given by eqn (55).

For $1/h = 15$ and $L/a \geqslant 15$, the numerical errors in Table 1 are less than 0.5%. For $1/h = 20$, the numerical results obtained stabilize as the plate size increases.

Based on the results shown in Table 1, it can be assumed that for $L/a \geqslant 10$, the boundaries of the solid lie, in a mathematical sense, at an infinite distance from the crack.

For each discretization shown in Table 1, the condition numbers [eqns (53) and (54)] of the system matrix (**A**) are in the range shown in Table 2.

For $1/h = 15$, the results in Table 1 are very accurate but the system matrix is ill conditioned, as shown in Table 2. For $1/h = 20$, the results in Table 1 are not as accurate as before ($1/h = 15$), but the system matrix is well conditioned with little variation in the condition number, as shown in Table 2.

Table 1. Error in K_{III} (%) as the size of the plate increases

L/a	5	10	15	20	25	30	35	40	45	50
$(1/h) = 15$	2.08	0.72	0.46	0.39	0.35	0.41	0.31	0.30	0.32	0.29
$(1/h) = 20$	4.29	2.88	2.62	2.53	2.49	2.47	2.46	2.45	2.44	2.44

Table 2. Condition numbers

$1/h$	$k(\mathbf{A})_{\min}$	$k(\mathbf{A})_{\max}$
15	9.4623×10^8	4.9308×10^{18}
20	882.20	882.67

For this example, the odd discretization ($1/h = 15$) gives more accurate results for the stress intensity factors than the even discretization ($1/h = 20$). However, all the problems using odd discretization were found to have very high condition numbers. Both $1/h = 15$ and $1/h = 20$ as well as $1/h = 50$ and $1/h = 100$ have been used in the numerical examples that follow.

It is possible that use of regularization (e.g. consideration of suitable constraint equations) would substantially reduce the condition numbers for the odd discretization examples above (Table 2). This is a topic for future research.

7.3. *Curved crack in an infinite body*

The purpose of this section is to investigate the influence of crack curvature and crack orientation on the stress intensity factors. Using the current definition of K_{III} [eqn (55)], the proposed method is compared with the analytical solution proposed by Sih (1965) for an infinite body loaded in anti-plane shear.

7.3.1. *Effect of crack curvature.* The graph in Fig. 9 illustrates the effect of crack curvature on the stress intensity factor. This graph has one point for each 0.1 increment in the parameter λ that describes the crack shape. For all the points in the graph, the absolute values of the SIF at the left and right crack tips are the same up to 4 decimal digits. Even discretization is used with $1/h = 20$. The condition number [eqn (53)] varies from 881.67 (for $\lambda = 5.0$) to 882.65 (for $\lambda = 0.0$).

The residue on the stress intensity factor is defined as

$$\text{Residue} = K_{III}(\text{BIEM}) - K_{III}(\text{Analytical}). \tag{58}$$

For this example, the analytical solution is available from Sih (1965). The residue in Fig. 9 decreases monotonically as the parameter λ increases. Using eqn (57), it can be verified that the relative error on K_{III} increases monotonically from 2.53% (for $\lambda = 0.0$) to 3.92% (for $\lambda = 5.0$). Note that K_{III} decreases with increasing λ.

Chiang (1987) has presented a solution for the SIF K_{III} for a slightly curved crack in an infinite body loaded in anti-plane shear based on earlier work for the in-plane loading case (Modes I and II) by Cotterell and Rice (1980). Chiang's results agree within 5% with Sih's analytical solution in Fig. 9 for $\lambda < 0.6$ (subtended angle $< 62°$). For $\lambda > 0.6$, the results diverge.

The accuracy of the method presented here can be verified by the good agreement between Sih's solution and the proposed one (BIEM), as illustrated by Fig. 9.

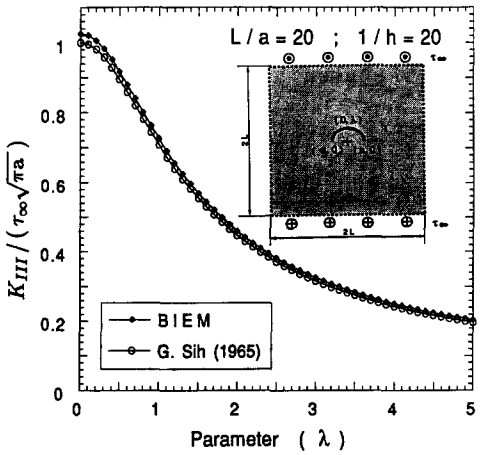

Fig. 9. Effect of crack curvature on the mode III SIF.

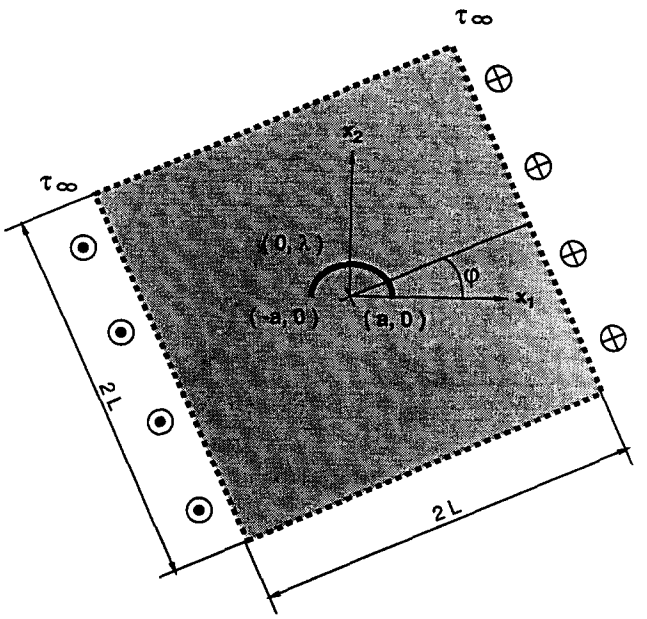

Fig. 10. Curved crack in a square plate of length $2L$.

7.3.2. *Effect of curved crack orientation.* In the previous example, $|K_{\text{III-R}}| = |K_{\text{III-L}}|$. In order to verify eqns (45) and (52), proposed for $K_{\text{III-R}}$ and $K_{\text{III-L}}$, respectively, the effect of curved crack orientation on the SIFs is considered next. In this example, a curved crack with $\lambda = 0.5$ is kept fixed and the outer boundary of the body (together with its boundary conditions) is rotated anticlockwise about the x_3 axis, as illustrated in Fig. 10. The analytical solution for this problem is available from Sih (1965).

An initial test is performed in order to assess the acceptability of the numerical discretization to be used for the present example. For this purpose, the previous example (Section 2.3.1) is used considering $\lambda = 0.5$ and an odd discretization with $1/h = 15$. The results are shown in Table 3.

Based on the results shown in Table 3, the odd discretization with $1/h = 15$ is adopted for the present example. The results are shown in Fig. 11. The condition numbers in this case varied from 1.1661×10^8 to 1.9649×10^{10}.

The graph in Fig. 11 shows that the BIEM and the analytical solutions agree perfectly within plotting accuracy.

7.4. *Symmetric edge effect*

The stress intensity factor formulae presented in eqns (45) and (52) are functions of crack geometry, applied load and geometry of the outer boundary ∂B. The previous example was based on the assumption that the crack is sufficiently far away from the outer boundary.

Table 3. Initial test for a body with a curved crack and odd discretization

Preliminary information	
λ (crack shape)	0.5
$1/h$ (uniform discretization)	15
K_{III} (G. Sih, 1965)/$(\tau_\infty\sqrt{\pi a})$	0.8944

Initial test	K_{III} (BIEM)/$(\tau_\infty\sqrt{\pi a})$	Error (%) [eqn (57)]
Right tip	0.8993	0.54
Left tip	−0.8967	0.26
k(A) [eqn (53)]	9.4622×10^8	

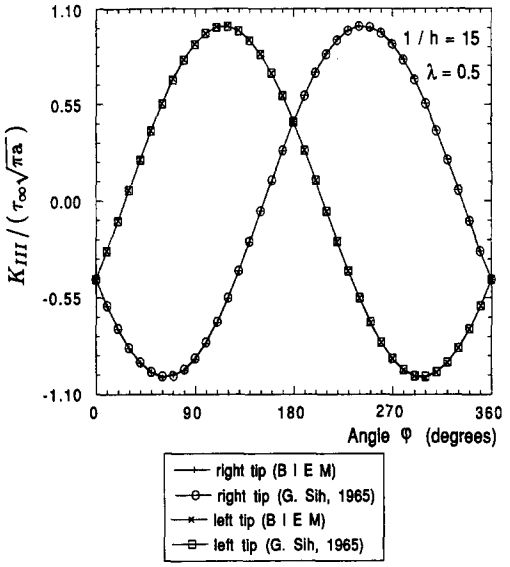

Fig. 11. Effect of curved orientation on the stress intensity factors $K_{III\text{-}R}$ and $K_{III\text{-}L}$.

However, the effect of a free boundary close to a crack causes the stresses to be higher than those of a crack in an infinite body, and therefore the stress intensity factor increases as a crack approaches a free boundary.

Two symmetric configurations are considered here: crack tips approaching perpendicular edges (i.e. a crack becoming progressively longer) and a crack approaching a parallel edge. Here, the notion of perpendicular or parallel edges is defined with respect to the crack line. The crack line is the line that connects the two tips of the crack.

Using the current definition of K_{III} [eqn (55)], the proposed method is compared with the analytical solution proposed by Ma and Zhang (1991) for an eccentric straight crack off the center line of a body with a rectangular cross-section. Ma and Zhang (1991) have expressed the stress intensity factor as a Fredholm integral equation of the second kind for situations where $|K_{III\text{-}R}| = |K_{III\text{-}L}|$.

7.4.1. *Crack tips approaching perpendicular edges.* This example shows the edge effect on the SIF as the crack tips approach the edges of a square plate that are normal to the crack line. A crack of length $2a$ is placed halfway between the top edge of the plate and the line parallel to the top edge, through the center of the plate. The crack length is varied in this example. The graph in Fig. 12 shows a comparison between the BIEM and the analytical

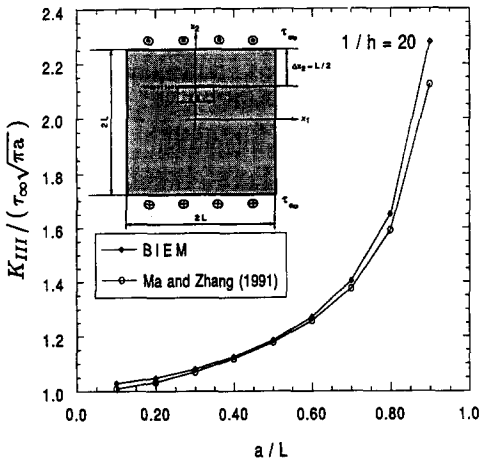

Fig. 12. Effect of the lateral edges on the mode III SIF.

Table 4. Uniform mesh enrichment for $(a/L) = 0.9$

$1/h$	K_{III} (BIEM)/$(\tau_\infty\sqrt{\pi a})$	Error (%) [eqn (57)]	$k(A)$ [eqn (53)]
20	2.279	7.35	869.11
30	2.231	5.09	1614.37
40	2.203	3.77	2499.47
50	2.186	2.97	3504.98
60	2.175	2.45	4617.85
70	2.167	2.07	5828.56
K_{III} (Ma and Zhang, 1991)/$(\tau_\infty\sqrt{\pi a}) = 2.123$			

solution from Ma and Zhang (1991). For $0.1 \leqslant (a/L) \leqslant 0.8$, the maximum relative error in K_{III} is 3.70%. For $(a/L) = 0.9$, the error is 7.35%. A larger error is expected for this case, since the crack tips are very close to the edges. However, this error can be greatly reduced by uniform enrichment of the boundary element mesh, as shown in Table 4.

The BIEM results in Table 4, for the SIF K_{III} considering $(a/L) = 0.9$ and even discretization, converge monotonically to the analytical solution of Ma and Zhang (1991). Moreover, the use of even discretization leads to a well conditioned system matrix, as shown in the last column of Table 4.

The graph in Fig. 12 and Table 4 demonstrate the accuracy of the numerical solution when compared to the analytical solution proposed by Ma and Zhang (1991).

7.4.2. *A crack approaching a parallel edge.* This example shows the edge effect on the SIF as a crack approaches the edge of a square plate that is parallel to the crack line, as illustrated by Fig. 13. This time, the crack length $2a$ is kept fixed.

Table 5 shows a comparison of the SIF K_{III} between the BIEM and the analytical solution from Ma and Zhang (1991).

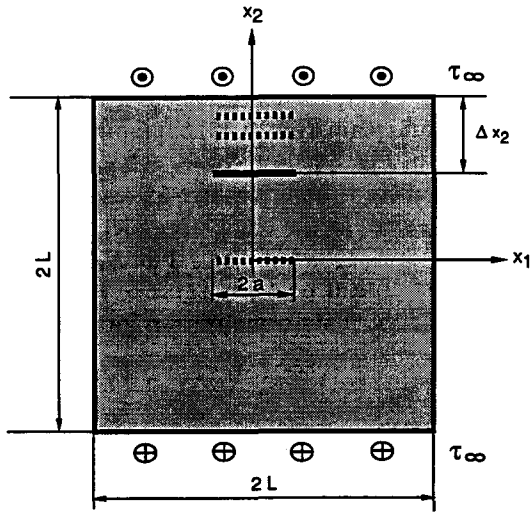

Fig. 13. Crack parallel to an edge of a square plate.

Table 5. Effect of a parallel edge on K_{III}

$\Delta x_2/L$	0.1	0.2	0.5	1.0
K_{III} (BIEM)/$(\tau_\infty\sqrt{\pi a})$	1.158	1.049	1.028	1.029
K_{III} (Ma and Zhang, 1991)/$(\tau_\infty\sqrt{\pi a})$	1.149	1.047	1.008	1.004
Error (%) [eqn (57)]	0.78	0.19	1.98	2.49
$k(A)$ [eqn (53)]	880.61	881.86	882.47	882.56
$a/L = 0.1$; $1/h = 20$				

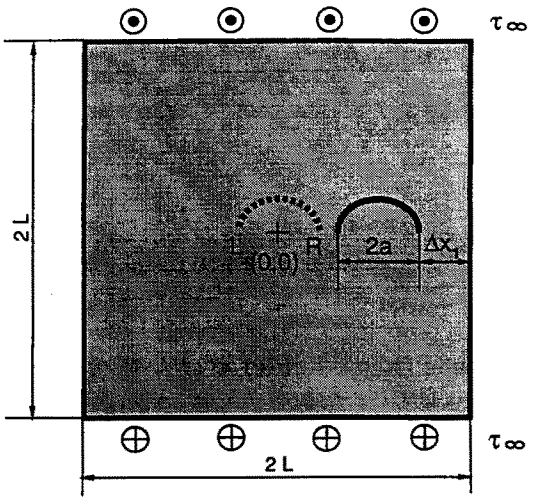

Fig. 14. Simulation of the nonsymmetric edge effect.

Table 5 shows that for $0.1 \leqslant \Delta x_2/L \leqslant 1.0$, the results for the SIF K_{III} are within 2.49% of the analytical solution. Moreover, the system matrix is well conditioned.

A comparison of the graph in Fig. 13 and the results in Table 5 reveals, as expected, that the proximity of a perpendicular edge to a crack tip has a larger influence on the SIF than the proximity of a parallel edge to a crack.

7.5. *Nonsymmetric edge effect*

This example shows the nonsymmetric edge effect in the SIFs $K_{III\text{-}R}$ and $K_{III\text{-}L}$ as the tips of a curved crack approach an edge that is perpendicular to the crack line, as illustrated in Fig. 14. No analytical solution is available for this problem.

In this example, a curved crack with $\lambda = 0.5$ is moved towards the right edge of the plate shown in Fig. 14. The results are shown in Table 6. Two normalizations for the SIFs are used in this table. The first one is with respect to the SIF for an infinite plate containing a straight crack, as in the previous examples. The second one is with respect to the analytical solution for the SIF for an infinite plate (Sih, 1965) containing a central curved crack with $\lambda = 0.5$, and loaded as shown in Fig. 14. For $\Delta x_1/L = 0.9$, the results from the last two columns of Table 6 show that there is an error of 1.65% in the numerical solution with discretization $1/h = 50$. As expected, as the crack approaches the right edge of the plate, both $K_{III\text{-}R}$ and $K_{III\text{-}L}$ increase with $K_{III\text{-}R}$ being larger than $K_{III\text{-}L}$ in all cases.

In order to verify the most critical point in Table 6, $(\Delta x_1/L = 0.1)$, a discretization $1/h = 100$ was used. Considering the first normalization for the SIF in Table 6, the results

Table 6. Effect of a perpendicular edge on $K_{III\text{-}L}$ and $K_{III\text{-}R}$

$\frac{\Delta x_1}{L}$	$\frac{K_{III\text{-}R}\ (\text{BIEM})}{\tau_\infty\sqrt{\pi a}}$	$\frac{K_{III\text{-}L}\ (\text{BIEM})}{\tau_\infty\sqrt{\pi a}}$	$\frac{K_{III\text{-}R}\ (\text{BIEM})}{K_{III\text{-}R}\ (\text{central crack})}$	$\frac{K_{III\text{-}L}\ (\text{BIEM})}{K_{III\text{-}L}\ (\text{central crack})}$
0.1	0.9608	0.9416	1.0742	1.0528
0.2	0.9286	0.9235	1.0382	1.0325
0.3	0.9194	0.9170	1.0279	1.0253
0.4	0.9152	0.9137	1.0232	1.0216
0.5	0.9127	0.9117	1.0204	1.0194
0.6	0.9111	0.9105	1.0187	1.0179
0.7	0.9101	0.9097	1.0175	1.0170
0.8	0.9095	0.9093	1.0168	1.0166
0.9	0.9092	0.9092	1.0165	1.0165

$a/L = 0.1$; $1/h = 50$

for the SIFs at the right and left crack tips are 0.9539 and 0.9357, respectively. These results are very close to the ones obtained with $1/h = 50$.

8. CONCLUSION

An efficient and accurate method for the stress analysis of an arbitrarily shaped, linearly elastic, homogeneous and isotropic body, with a curved crack loaded in anti-plane shear, has been presented in this paper. The effect of the crack on the stress field is incorporated in an augmented kernel developed for the mode III fracture mechanics problem such that discretization of the crack boundary is not necessary. The symmetric mapping property, defined in Section 4, is important for the accuracy of the solution.

An asymptotic analysis has been conducted to derive contour integrals for the stress intensity factors at the left and right crack tips, $K_{\text{III-L}}$ and $K_{\text{III-R}}$, respectively. These integral equations require far field boundary data, available from a numerical solution of the boundary value problem [eqn (8)], without any special treatment of the crack surfaces, as is usually done in multidomain modeling using boundary elements (Blandford *et al.*, 1981); and also without any special treatment of the region surrounding the crack tips, as is usually done when the finite element method is used (Owen and Fawkes, 1983).

Several numerical examples, for straight and curved cracks, have been presented in this paper. Some examples simulate plates that are of infinite extent relative to the crack size, while others investigate the effect of plate edges that are in close proximity of a crack. The BIEM results show excellent agreement with analytical solutions whenever the latter are available.

Acknowledgements—The first author would like to acknowledge the financial support provided by the CNPq (National Council for Research and Development) Brazilian Agency. Professor Subrata Mukherjee's contribution to this research was supported by grant number MSS-8922185 of the National Science Foundation to Cornell University. The authors would like to acknowledge valuable suggestions from Professors Clifford Earle and Lars B. Wahlbin, Department of Mathematics, and Professor John F. Abel, School of Civil and Environmental Engineering, all of them from Cornell University.

REFERENCES

Blandford, G. E., Ingraffea, A. R. and Ligget, J. A. (1981). Two-dimensional stress intensity factor computations using the boundary element method. *Int. J. Numer. Meth. Engng* **17,** 387–404.

Chiang, C. R. (1987). Slightly curved cracks in antiplane strain. *Int. J. Fract.* **32,** R63–R66.

Cotterell, B. and Rice, J. R. (1980). Slightly curved or kinked cracks. *Int. J. Fract.* **16**(2), 155–169.

Dettman, J. W. (1984). *Applied Complex Variables.* Dover, New York.

Erdélyi, A. (1956). *Asymptotic Expansions.* Dover, New York.

Freund, L. B. (1990). *Dynamic Fracture Mechanics.* Cambridge University Press, Cambridge.

Ghosh, N. (1982). On the Convergence of the Boundary Element Method. PhD Thesis, Department of Mathematics, Cornell University, Ithaca, NY, U.S.A.

Golub, G. H. and Van Loan, C. F. (1989). *Matrix Computations* (2nd Edn). The Johns Hopkins University Press, Baltimore and London.

Greenberg, M. D. (1978). *Methods of Applied Mathematics.* Prentice Hall, Englewood Cliffs, NJ.

Liu, N. and Altiero, N. J. (1992). An integral equation method applied to mode III crack problems. *Engng Fract. Mech.* **41**(4), 587–596.

Liu, N., Altiero, N. J. and Sur, U. (1990). An alternative integral equation approach applied to kinked cracks in finite plane bodies. *Comput. Meth. Appl. Mech. Engng* **84,** 211–226.

Ma, S. W. (1988). A central crack in a rectangular sheet where its boundary is subjected to an arbitrary anti-plane load. *Engng Fract. Mech.* **30**(4), 435–443.

Ma, S. W. and Zhang, L. X. (1991). A new solution of an eccentric crack off the center line of a rectangular sheet for mode-III. *Engng Fract. Mech.* **40**(1), 1–7.

Mews, H. and Kuhn, G. (1988). An effective numerical stress intensity factor calculation with no crack discretization. *Int. J. Fract.* **38,** 61–76.

Mukherjee, S. (1982). *Boundary Element Methods in Creep and Fracture.* Applied Science Publishers, London and New York.

Muskhelishvili, N. I. (1963). *Some Basic Problems of the Mathematical Theory of Elasticity.* Noordhoff, Groningen, The Netherlands.

Owen, D. R. J. and Fawkes, A. J. (1983). *Engineering Fracture Mechanics: Numerical Methods and Applications.* Pineridge Press, Swansea, U.K.

Rice, J. R. (1968). Mathematical analysis in the mechanics of fracture. In *Fracture—An Advanced Treatise* (Edited by H. Liebowitz), Vol. II, pp. 191–311. Pergamon Press, Oxford.

Sadegh, A. and Altiero, N. J. (1979). Solution of the problem of a crack in a finite plane region using an indirect boundary-integral method. *Engng Fract. Mech.* **11,** 831–837.

Schinzinger, R. and Laura, P. A. A. (1991). *Conformal Mapping: Methods and Applications*. Elsevier Science Publishers, Amsterdam.
Sih, G. C. (1965). Stress distribution near internal crack tips for longitudinal shear problems. *J. Appl. Mech.* **32,** 51–58.
Sloan, I. H. (1991). Error analysis of boundary integral methods. *Acta Numer.* 287–339.
Zang, W. and Gudmundson, P. (1988). A boundary integral method for piece-wise smooth crack problems. *Int. J. Fract.* **38,** 275–294.
Zhang, X. S. (1987). The general solution of a central crack off the center line of a rectangular sheet for mode III. *Engng Fract. Mech.* **28**(2), 147–155.
Zhang, X. S. (1989). A tearing mode crack located anywhere in a finite rectangular sheet. *Engng Fract. Mech.* **33**(4), 509–516.

APPENDIX: DEFINITION OF STRESS INTENSITY FACTORS

The purpose of this appendix is to define the stress intensity factor $K_{\text{III-L}}$ at the left crack tip. For this purpose, a crack in the center of a plate is considered as shown in Fig. A1. The plate is loaded in anti-plane shear and the crack is straight.

Using local polar coordinates r and θ at the right crack tip (Figs 5 and A1), it is well known that:

$$\sigma_{3r}(\mathbf{A}) = \frac{K_{\text{III-R}}}{\sqrt{2\pi r}} \sin\left(\frac{\theta}{2}\right), \tag{A1}$$

$$\sigma_{3\theta}(\mathbf{A}) = \frac{K_{\text{III-R}}}{\sqrt{2\pi r}} \cos\left(\frac{\theta}{2}\right). \tag{A2}$$

Now let the plate be rotated by 180° about the x_3 axis and the sign of the remote loading τ_∞ be charged, as illustrated by Fig. A2. This leads to the following equations:

$$\sigma_{3r}(\mathbf{A}') = -\frac{K_{\text{III-R}}}{\sqrt{2\pi r}} \sin\left(\frac{\theta}{2}\right), \tag{A3}$$

$$\sigma_{3\theta}(\mathbf{A}') = \frac{K_{\text{III-R}}}{\sqrt{2\pi r}} \cos\left(\frac{\theta}{2}\right), \tag{A4}$$

in terms of the local polar coordinates r and θ defined in Fig. A2.

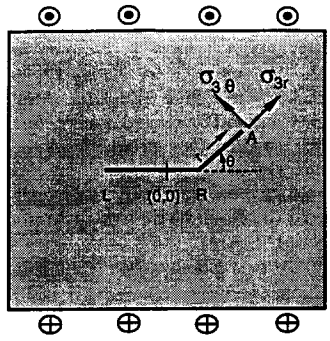

Fig. A1. Reference plate.

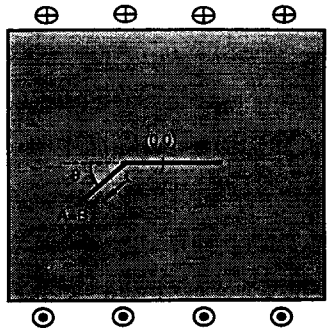

Fig. A2. Rotated plate.

Finally, $K_{\text{III-L}}$ is defined in this symmetric case as:

$$K_{\text{III-L}} = -K_{\text{III-R}}, \tag{A5}$$

such that

$$\sigma_{3r}(B) = \frac{K_{\text{III-L}}}{\sqrt{2\pi r}} \sin\left(\frac{\theta}{2}\right), \tag{A6}$$

$$\sigma_{3\theta}(B) = \frac{K_{\text{III-L}}}{\sqrt{2\pi r}} \cos\left(\frac{\theta}{2}\right), \tag{A7}$$

which are of the same form as eqns (A1) and (A2). The general formula for $K_{\text{III-L}}$ is given in eqn (52).